



Experimental and Analytical Study on the Shear Transfer in Composite Post Tensioned Precast Concrete Girders

Wael Nabil^{1,2} · Ibrahim G. Shaaban³ · Ayman Khalil¹ · Sherif Elwan²

Received: 10 January 2023 / Revised: 22 June 2023 / Accepted: 13 July 2023 / Published online: 3 August 2023
© Crown 2023

Abstract

This paper proposes a new system for constructing composite post-tensioned precast concrete girders with top slabs where the bottom part is precast, and the top part is cast in place. The experimental study consisted of testing six composite T-girders under two-point loading. The first specimen is post tensioned T-section cast monolithically and acts as a control specimen. In the other five specimens, the web and the girder flange were poured separately and then connected. The investigated variables are the shear connectors' distribution, extended girder stirrups acting as shear connectors, the top slab width, and the concrete strength of the top slabs. Available models from the literature and international code provisions are used for calculating shear transfer failure loads. Based on the obtained results, an analytical study was conducted based on the available model results. This was done to determine the most accurate correlation with the experimental results. The test results showed that using the shear connectors or full stirrups to connect the top slabs to the girders could achieve the total capacity of the monolithic girder. Using shear connectors of 10 mm diameter achieved 100% of the monolithic T-section girder, while using shear connectors of 12 mm diameter achieved 105%. Extending girder stirrups to connect the top slabs to the girders instead of using the shear connectors achieved 100% of the capacity. In addition, increasing the slab width by 50% improved the ductility of the composite T-girders and increased the capacity of the girder by 3%. Moreover, using lower concrete strength for slabs increases slippage between slabs and girders and decreases ultimate girder capacity by 15%. Comparisons between the theoretical results obtained by the available models, codes provisions, and experimental results were made, and conclusions were drawn. The comparisons showed that the Loov's equation is the least conservative value with the experimental results.

Keywords Post tensioned · Composite concrete girders · Precast concrete · Shear connector · Horizontal shear

1 Introduction

Composite precast concrete is widely used in bridge construction. It can achieve all structural requirements, including decreasing overall mobilization, increasing construction speed, and maintaining high-quality control [1, 2]. The prevailing concept is a deck made almost entirely of prefabricated pieces, such as a full-depth precast bridge deck system [3, 4]. Full-depth precast concrete decks are manufactured composite by connecting the deck panels to the supporting beams using different types of shear connections, such as shear studs, bent bars, or threaded rods with nuts [5, 6]. These connections are fixed into concrete beams through fabrication or welded to the top flange of the steel beam before or after placing the precast concrete deck slabs [4]. Due to the self-heavy weight and worse

✉ Ibrahim G. Shaaban
ibrahim.shaaban@uwl.ac.uk

Wael Nabil
w.nabil@sha.edu.eg

Ayman Khalil
ayman.hussein.khalil@eng.asu.edu.eg

Sherif Elwan
S.elwan@sha.edu.eg

¹ Structural Engineering Department, Faculty of Engineering, Ain Shams University, Cairo, Egypt

² Civil Engineering Department, The Higher Institute of Engineering, El Shorouk Academy, Cairo, Egypt

³ School of Computing and Engineering, University of West London, London W5 5RF, UK

tensile strength of normal concrete girders, the full depth precast concrete decks were mainly applied for bridge with steel girder become among the current investigations [7–9]. The disadvantage of this system is that it requires larger quantities of grout material to fill the shear pockets and shear keys [6].

Throughout the years, researchers reported that the behaviour of the interface between the web and the topping slab (flange) of the composite girder affects girder behaviour significantly, as horizontal shear behaviour is crucial for the development of diagonal shear strength, deflection behaviour, and flexural strength to achieve monolithic action [3, 10]. The horizontal shear strength of a composite girder mainly depends on the ratio of reinforcement crossing the interface. It also depends on the interface type between the web and flange, and the concrete strength [10–13]. Therefore, shear connectors are required to resist the horizontal shear at the interface surface so that the concrete web and flange act as one unit. Figure 1 illustrates horizontal shearing forces in a composite section [14].

As resisting horizontal shearing forces develop in the girder and the slab, there is little relative slip between the two surfaces. This may happen due to small cracks along the two interfaces. As the relative slip happens, the shear connectors protruding from the girder into the slab develop tensile forces. They lead to compressive forces through the interface zone and act as horizontal shearing forces. Horizontal shearing forces are transported between the two surfaces by friction due to compressive forces and reinforcement crossing the interface [15]. Figure 2 shows the interface forces developed between the two surfaces due to relative slip [16].

Several research studies studied the interfacial shear behaviour between ultra-high-performance concrete and normal strength concrete in precast composite members [17–19]. They reported that the shear resistance of the interface was improved by increasing the concrete strength and the degree of surface roughness. They also found that shear reinforcement crossing the interface significantly reduced interface slip before failure. Other researchers studied horizontal shear behaviour between lightweight concrete and normal-weight concrete in concrete composite members [10, 20]. They reported that the preparation

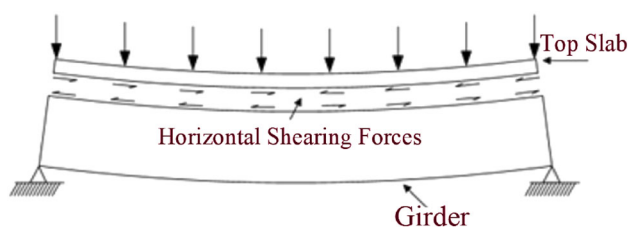


Fig. 1 Horizontal shearing forces in a composite section [14]

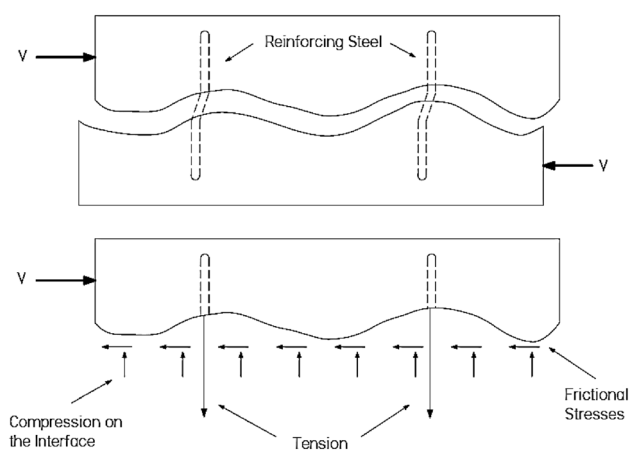


Fig. 2 Interface forces between the two surfaces [16]

method of the interface, clamping stress, and the slab's concrete strength substantially affected interface slippage at failure. They also reported that most composite girders failed in horizontal shear due to horizontal cracks along the interface and separation between the web and the flange.

The distribution of shear connectors is crucial. Throughout the years, there have been many studies and proposed equations to determine the horizontal shear strength of the interface zone in composite sections. Mast was the first to introduce a linear shear friction equation [21]. Birkeland and Birkeland introduced a non-linear function for the ultimate shear capacity of the interface, Birkeland's equation only incorporated a factor times the clamping stress, and nothing accounted for varying surface treatment or concrete strength [22]. Mattock and Hawkins presented a design expression to predict the ultimate longitudinal shear stress and represented the lower bound of the experimental tests. In their previous equation, they reintroduced the concrete strength effect. They also investigated horizontal shear strength for lightweight concrete members [23]. Shaikh proposed a modification to ACI's shear-friction provisions [24], these modifications were incorporated in ACI code 318 [25]. Loov introduced concrete strength influence into the horizontal shear strength equation [26]. Patnaik performed 24 beam tests to study the adequacy of the ACI building code [25] with respect to horizontal shear with a smooth interface. Patnaik stated that it is possible to obtain some nominal shear strength from a smooth interface with no reinforcement, but for design this is not recommended [27].

From the above literature, many researchers studied the behaviour of composite precast concrete members by using several parameters such as the interface surface type, changing the concrete strength by utilizing ultra-high-performance concrete or lightweight concrete, and the ratio of reinforcement crossing the interface. These were carried out for the traditional composite girder systems, which

usually consists of a precast beam with a cast-in-place slab [12, 13] or a full-depth precast concrete panel system [3–6]. This research proposed a new system for composite precast concrete T-girders. It investigated the behaviour of this system by using several parameters on which no research was cited, such as the combined effects of different shear connector distributions, applying full stirrups to connect the top slab with a supporting beam, changing the top slab width, and changing the compressive concrete strength of top slabs.

2 Objective and Research Significance

This study proposes a new system for composite post tensioned concrete girders with top slabs where the slab's bottom part is precast concrete, and its top part is cast-in-place concrete, as shown in Fig. 3. The girders and slabs are cast in the controlled environment of a precast yard prior to construction. They are transferred separately to decrease weight during transport and lifting. Formwork or grout injection will be saved. In addition, there are no large quantities of concrete to be laid and processed on site. This will improve the quality of the concrete and speed up the construction process. All the above factors provide a higher quality product while reducing traffic interruptions. Figure 4 shows a flowchart for research.

3 Experimental Program

3.1 Specimen Details

The experimental program consisted of testing six specimens. The investigated variables are the shear connectors' distribution, extended girder stirrups acting as shear connectors, the top slab width, and the concrete strength of the top slabs. The girder bottom reinforcement was 2D16 mm diameter bars, and the top reinforcement was 2D12 mm

diameter bars with a concrete cover of 25 mm. The flange reinforcement was D10 @ 200 mm in both directions. All the specimens were post-tensioned using two prestressing tendons with a 15.24 mm diameter. We reinforced the specimens with closed stirrups of D8 @ 100 mm on the first 500 mm and 125 mm spacing on the remainder. Special reinforcement at the end zones was provided to prevent splitting and bursts.

Specimen (G1) was cast monolithically and considered a control specimen. Table 1 lists specimen details, and the dimensions are shown in Fig. 5. For the rest of the specimens, girder webs and the lower part of topping slabs were cast first separately. Then, the lower part was installed on the girder web, and the rest of topping slab was cast in place. The reinforcement of the bottom and top parts of the slab was D10 @ 200 mm in both directions. Dimensions are shown in Fig. 6, and specimens' preparations are shown in Figs. 7, 8, 9, 10, 11, 12, 13, 14 and 15. For all six specimens, post tensioning was applied first.

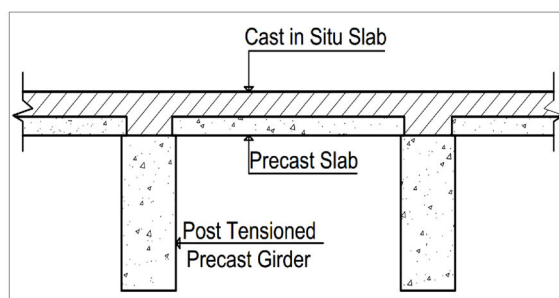
In Specimen G2, the shear connectors are D10 @ 161 mm, while in Specimen G3, the shear connectors are D12 mm @ 233 mm. In the fourth Specimen (G4), the shear connectors are replaced by full stirrups. The fifth Specimen (G5) is similar to Specimen G2, but the slab width is 750 mm instead of 500 mm. The sixth specimen (G6) is similar to Specimen G2, but the compressive concrete strength for the top slabs is 25 MPa instead of 40 MPa.

3.2 Material Properties

The concrete's designed cube compressive strength was 40 MPa after 28 days. The concrete mix proportion for 40 MPa was 1124 kg/m³ (coarse aggregates), 630 kg/m³ (fine aggregates) and 3.5 L/m³ (Super plasticizer). The water/cement ratio was 0.46, and the cement content was 400 kg/m³. The concrete mix proportion for 25 MPa was 1200 kg/m³ (coarse aggregates) and 800 kg/m³ (fine aggregates). The water/cement ratio was 0.5, and the



Fig. 3 Structural system



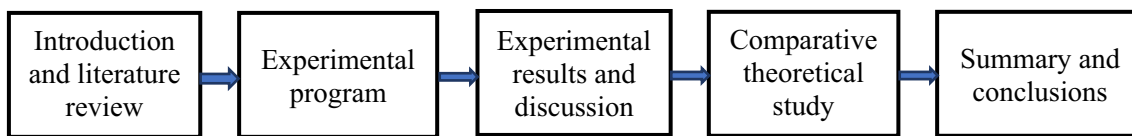


Fig. 4 Flowchart for research

Table 1 Details of test specimens

Girder ID	Description of shear connectors	Shear connectors ratio (%)	Top slab width (mm)	f_{cu} of web girder (MPa)	f_{cu} of slabs (MPa)
G1	Monolithic construction	–	500	40	40
G2	Ø10@161 mm (26 Ø10)	0.405	500	40	40
G3	Ø12@233 mm (18 Ø12)	0.405	500	40	40
G4	Full stirrups (Ø8@125 mm)	0.698	500	40	40
G5	Ø10@161 mm (26 Ø10)	0.405	750	40	40
G6	Ø10@161 mm (26 Ø10)	0.405	500	40	25

cement content was 350 kg/m^3 . Each specimen was cast in one batch. The reinforcement was high tensile steel with a minimum proof strength of 400 MPa for D10 or more. It was also mild steel with a minimum yield strength of 240 MPa for D8. High-grade steel strands of 15.24 diameter comprising seven individual wires were used. The ultimate tensile strength and the elastic modulus of the steel strands were 1860 MPa and 195000 MPa, respectively. Figure 16 shows the stress-strain diagram of the materials.

3.3 Load Setup, Test Procedure, and Instrumentation

The test setup consisted of a structural steel loading frame fixed to a rigid floor. The girders were supported by hinges, and from the other side, by rollers. These supports rested on steel columns anchored to the floor. One load cell of 1000 kN capacity was used during the test. The load was distributed using a rigid steel beam at two concentrated points, as shown in Fig. 17. During testing, loading was paused at different load levels to visually inspect the girders for cracks. Cracks were marked on the specimen's surface. Displacements were monitored using linear variable displacement transducers (LVDTs). Figure 18 shows the locations of the LVDTs and strain gauges for a typical girder. The deflection was monitored at three locations, and relative vertical and horizontal movement was monitored at four locations. The steel reinforcement strain was measured by electrical strain gauges. Deflection and strain readings were recorded automatically during the test, using a data acquisition system at each load increment.

4 Experimental Results

The load at first crack and the failure loads were recorded, and the relationship between failure loads and deflection values was drawn. Table 2 summarized the cracking and failure load for all tested specimens.

4.1 Crack Pattern and Failure Mode

Figures 19 and 20 show the tested girders' cracking patterns and failure modes. In control Specimen G1, the cracks initiated at the mid-span of the girder web increased in number and width by increasing the load up to failure. Horizontal cracks appeared at the web and flange interfaces for all composite girders. The failure in specimens G3 and G4 was due to tensile flexure. Many horizontal cracks with smaller widths appeared at the interface between the web and the flange. However, the vertical cracks widened at the mid-span of the girder web, and the top flange was crushed, as shown in the figures. In specimens G2 and G6, the horizontal cracks increased in number and width, leading to failure due to slippage between the web and flange at the end girder. In addition, many vertical cracks with smaller widths were present at the girder web mid-span. In Specimen G5, which had a wider slab, many horizontal cracks with smaller widths appeared at the interface between the web and the flange. However, the failure occurred flexibly followed by crushing at the compression flange. This seems to agree with researchers in the literature who observed similar crack propagation in their experimentally studied composite prestressed concrete girders [10, 11, 27].

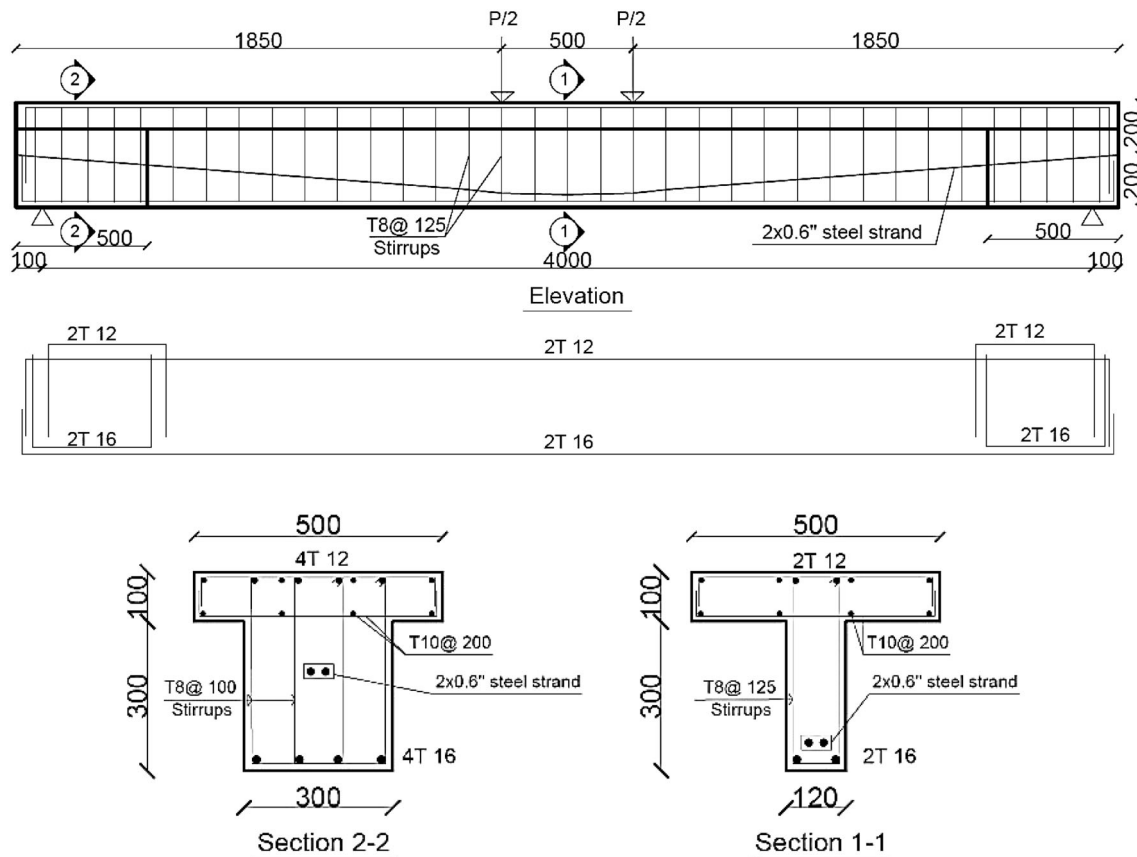


Fig. 5 Details of control specimen (G1)

4.2 Failure Load and Deformations

Figures 21 and 22 show the relationship between loads and vertical deflections. All girders pass through three stages. At each of the three stages, the load–deflection relation slope changes. The first stage is pre-cracking, where the relation between the load and vertical deflection varies linearly. At Stage Two, where the relation varies linearly and the slope changes due to the loss of sectional stiffness by cracking, the loss of stiffness is constant until the yielding point of strands is reached. Finally, at Stage Three or the plastic phase, the slope of the relationship is reduced due to yielding and the wide cracks until the failure point. The ductility index is the ratio between the deflection at the ultimate load and the deflection measured when the steel reaches yield strain.

The ultimate load of specimen G2 is the same as that of control specimen G1. At the same time, the ductility index and maximum deflection of specimen G2 are lower than those of control specimen G1 by 16.48% and 3.88%, respectively. It can be noted that using shear connectors 10 mm in diameter almost achieved the same results as the control specimen.

The ultimate load of specimen G3 is greater than specimens G1 and G2 by 5.45%. The ductility index and maximum deflection of specimen G3 are lower than specimen G1 by 19.1% and 6.86%. They are also lower than specimen G2 by 3.13% and 3.1%, respectively. This can be attributed to using shear connectors 12 mm in diameter, increasing the stiffness of specimen G3 compared to the control specimen.

The ultimate load and ductility index of specimen G4 is lower than those of control specimen G1 by 1% and 4.87%, respectively. The maximum deflection of G4 is higher than that of the control specimen by 4.48%. In addition, the ultimate load of Specimen G4 is lower than Specimens G2 and G3 by 1% and 6.03%, respectively. The ductility index and maximum deflection of Specimen G4 are higher than those of G2 by 13.9% and 8.7%, and higher than those of G3 by 17.6% and 12.18%, respectively. It can be noted that extending girder stirrups to connect the top slabs to the girder instead of using shear connectors almost achieved similar results to the control specimen.

In specimen G5, which had a wider slab of 750 mm instead of 500 mm, the ultimate load is higher than that of G2 by 3.03%. In addition, the ductility index and maximum deflection of G5 are higher than G2 by 12.11% and

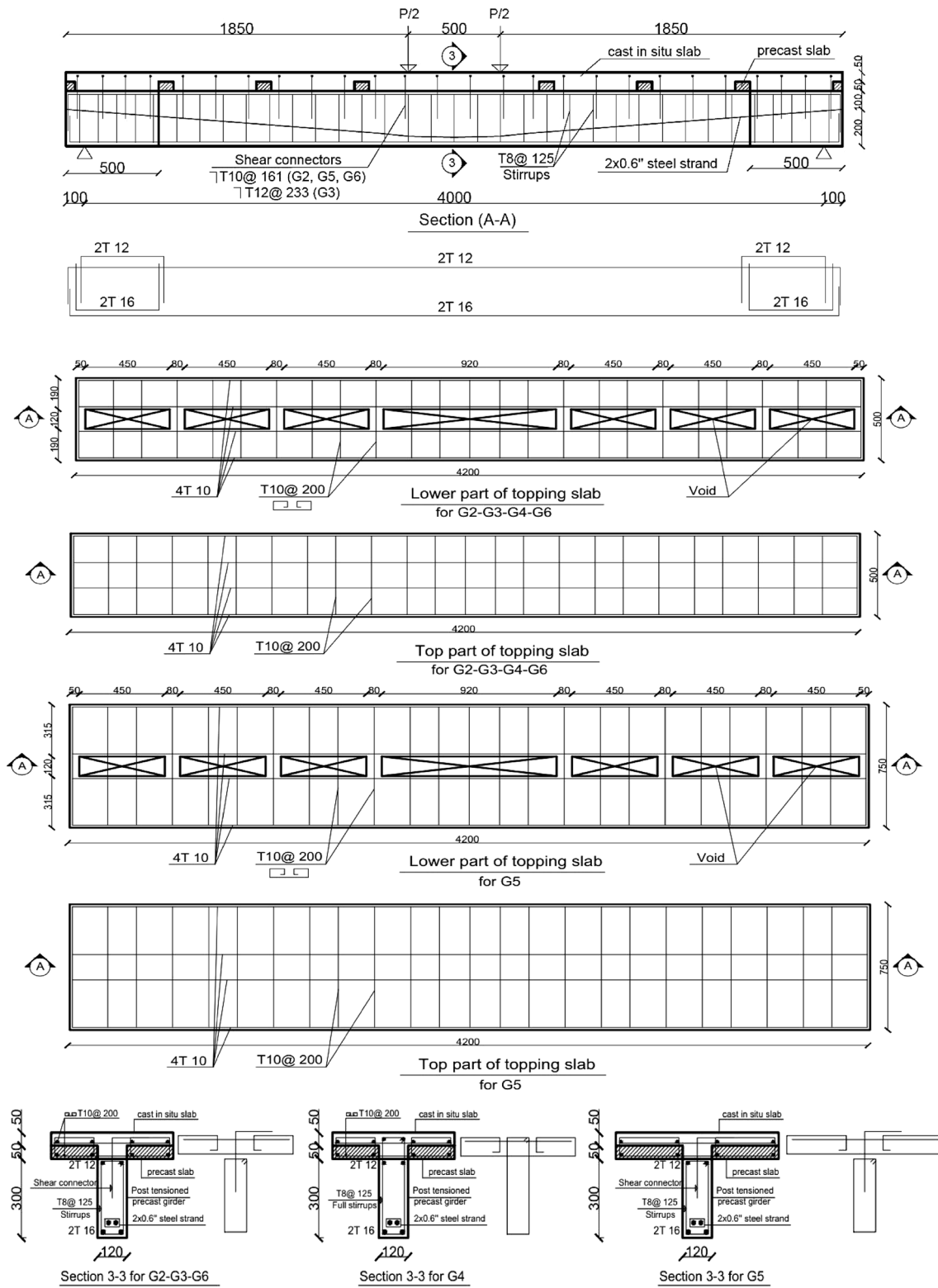


Fig. 6 Details of specimens (G2–G6)

4.03%, respectively. This can be attributed to the increasing stiffness of specimen G5 due to the increasing slab width compared to the control specimen.

Specimen G6, which had a lower concrete strength for the top slabs of 25 MPa instead of 40 MPa, the ultimate load is lower than that of G2 by 14.54%. However, it



Fig. 7 Preparation of formwork for tested specimens

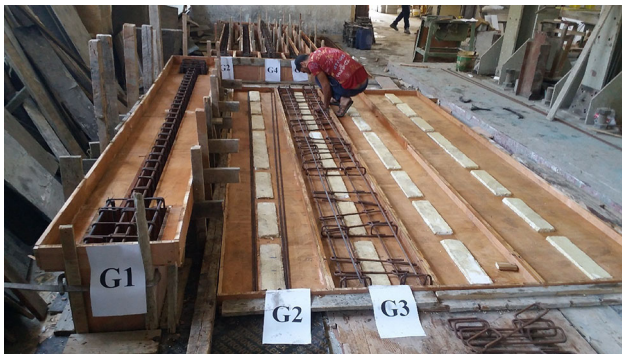


Fig. 8 Preparation of reinforcement for tested specimens

achieved a higher ductility index and maximum deflection than G2 by 11.21% and 10.25%, respectively. This can be attributed to the composite girder’s horizontal shear strength. This mainly depends on the concrete strength at the interface compared to the control specimen.

Again, the ultimate loads, deflections, and ductility were similar to those observed by other researchers in the literature who studied composite girders [10, 11, 27].

Figure 23 shows the relative horizontal displacement between the web and the slab. The girder with lower concrete strength for the top slabs (G6) experienced more relative horizontal displacement than the other girders due to the shear resistance of the interface in the composite girders depending on concrete strength. The reinforcing bars across the interface were ineffective in this case for providing the maximum shear resistance and rigidity prior to the slip. This seems to agree with the researchers who studied the effect of changing concrete strength in their study. They found that the mechanical bonding strength



Fig. 9 Finishing preparation of reinforcement for all specimens



Fig. 10 Control specimen G1 and five girder webs



Fig. 11 Lower part of topping slab (precast)

and shear resistance of the interface increased by increasing the concrete strength of slab [10, 17–20].

For girders with the same area of shear connectors (G2 and G3), G2 experienced more relative horizontal displacements than G3. This may be attributed to the higher stiffness of the 12 mm bars, which governs girder



Fig. 12 Installation of the lower part of topping slab above girder web



Fig. 13 Preparation of casting the rest of topping slab



Fig. 14 Casting concrete for the rest of topping slab (G2–G6)



Fig. 15 Finishing casting concrete for the rest of topping slab (G2–G6)

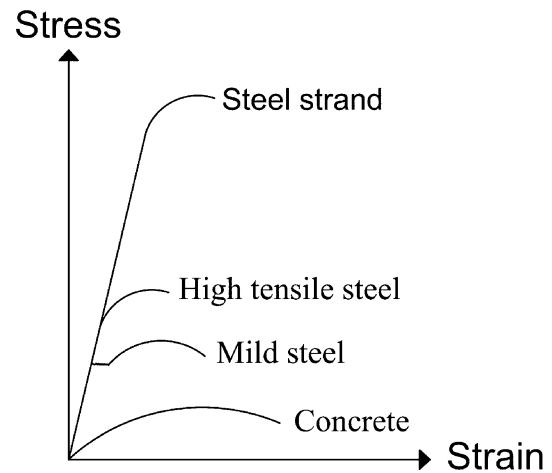


Fig. 16 Stress- strain diagram of the materials

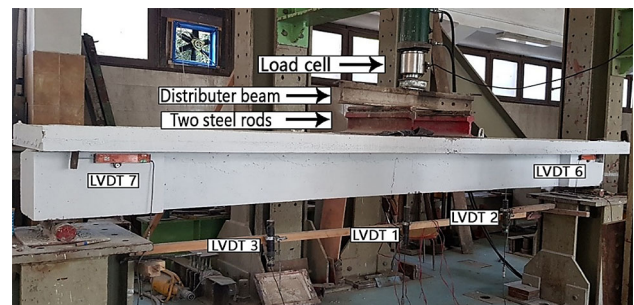


Fig. 17 Test set-up for the girders

behaviour. Specimen G5, which had a wider slab, experienced less relative horizontal displacement at the interface than specimen G2. This may be attributed to the high stiffness of the wide flange. This decreases slab deflection and relative horizontal displacement.

4.3 Failure Load and Strain

Figure 24 shows the relationship between the load and the longitudinal steel strains measured at the mid-span. It can be noticed that the maximum steel strain is almost the same for all girder specimens due to the same reinforcement ratio, the strain prior to interface cracking was close to the yield strain.

Figures 25a–f show the strain distribution through the cross-section depth at different loading levels for each specimen. The strain distribution was drawn by connecting SG1, SG3, and SG4 readings in specimen G1. For the rest of the specimens, the neutral axis was determined at different loading levels by measuring the crack length from the experimental work. The neutral axis was assumed above the end of crack. Then a line was plotted from SG1 to the neutral axis and extended to the end of the web girder. A line was plotted from SG3 to SG4.

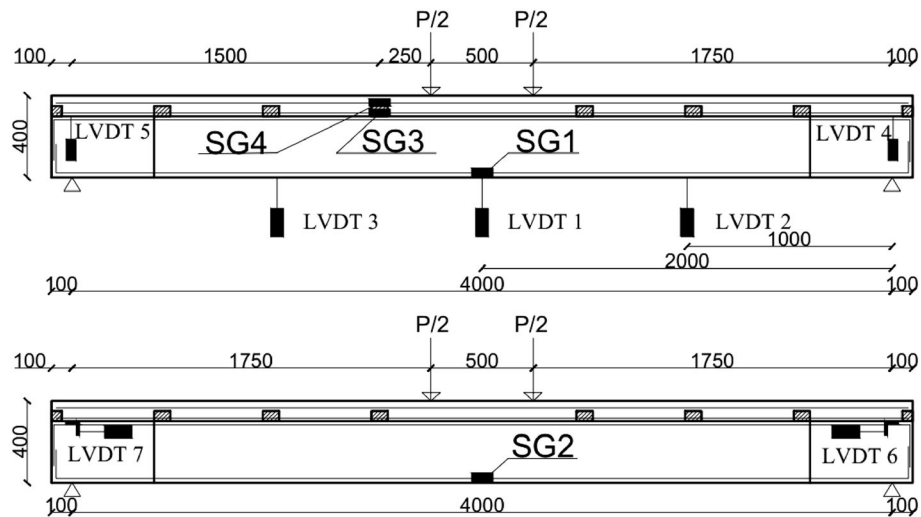


Fig. 18 Instrumentation for the girders

Table 2 Summary of experimental results for all tested girders

Girder ID	First crack load (kN)	Load at first interfacial crack (kN)	Failure load (kN)	Deflection at steel yield (LVDT1) (mm)	Max. deflection (LVDT1) (mm)	Ductility index	Max. strain (SG1)	Failure mode shape
G1	70	–	330	25.10	67	2.67	0.019135	Flexure followed by crushing at the compression flange
G2	100	210	330	28.88	64.4	2.23	0.019500	The slippage between web and flange at the end girder accompanied by flexure cracks
G3	80	200	348	28.89	62.4	2.16	0.019299	Flexure followed by crushing at the compression flange, accompanied by cracks between web and flange at the end girder
G4	70	210	327	27.56	70	2.54	0.019355	Flexure followed by crushing at the compression flange, accompanied by cracks between web and flange at the end girder
G5	70	190	340	26.80	67	2.5	0.019055	Flexure followed by crushing at the compression flange, accompanied by cracks between web and flange at the end girder
G6	70	190	282	28.63	71	2.48	0.019519	The slippage between web and flange at the end girder accompanied with flexure cracks

It can be seen from Fig. 18 that, for all composite girders except G6, the strain distribution was almost continuous at the interface of the web and the slab, especially at the early stages of loading, which indicating full shear interaction between the web and slab. However, as the load increased, the small cracks at the interface were due to the relative slip between the web and slab. The discontinuity of the strain at the interface became more pronounced, indicating a partial shear interaction. It can be concluded that

all composite girders except Specimen G6, almost have full composite action. This is in agreement with Wang, who observed that the strain distribution through the depth of cross-section is linear at the stage before the cracks load, and it subsequently became nonlinear because of the cracks emerging by increasing the load [20].

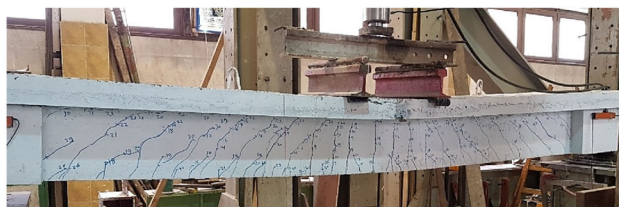
For Specimen G6, the strain distribution at the early stages of loading is almost continuous, indicating full shear interaction between the web and slab. However, as the load



a) Specimen G1



b) Specimen G2



c) Specimen G3



d) Specimen G4



e) Specimen G5



f) Specimen G6

Fig. 19 Cracking patterns of tested specimens

increased, the relative slippage between the web and the flange occurred, then the two members acted as a non-composite section and resisted the load as two separate members.

5 Comparative Theoretical Study

Horizontal shear strength values were calculated using available models from the literature and codes provisions. Many proposed equations have been developed to determine the horizontal shear strength of the interface zone in composite sections. A summary of the variables considered in the equations of codes provisions and models is presented in Table 3. It can be noticed that all codes provisions and model equations consider clamping stress. It can also be noticed that AASHTO LRFD2010 [28], Eurocode-2 [29], ECP 203–2020 [30], Mattock [23] and Patnaik [27] take into account cohesion. In addition, Loov's model [26] is the only equation based on reinforcement strength and concrete. Where f_c is the cylindrical concrete strength, f_y is the reinforcement yield strength, ρ_v is the ratio of the steel crossing interface (shear connectors ratio) $= (A_{vf}/A_c)$, where A_{vf} is the area of reinforcement crossing interface (shear connectors area) and A_c is the area of the cracked interfacial surface. $\rho_v = 0.405\%$ for specimens G2, G3, G5, G6, and $\rho_v = 0.698\%$ for specimens G4. μ is the coefficient of friction at the interface, which depend on the interface's roughness.

C is the cohesion factor which depends on the roughness of the interface.

Table 4 compares the experimental results and the interfacial shear failure loads calculated from previous research in the literature and design codes. Figure 26 summarises the experimental results and the interfacial shear failure loads calculated from the analytical study. It was found that the equations of Mast [21], BS 8110 [31], Eurocode-2 [29], ECP 203–2020 [30], and Patnaik [27] are conservative for determining the horizontal shear stress due to the conservative values for cohesion and interfacial friction. Mattock [23] and Shaikh [24]'s equations are less conservative for determining the horizontal shear stress due to the high contribution of cohesion and friction in those equations. In this case, Loov [26], Birkeland [22], and AASHTO LRFD [28] represent the least conservative equation.

The proposed equations are as follows:

- Mast equation [21]

$$V_n = \rho_v f_y \mu \quad (1)$$

where $\mu = 1$

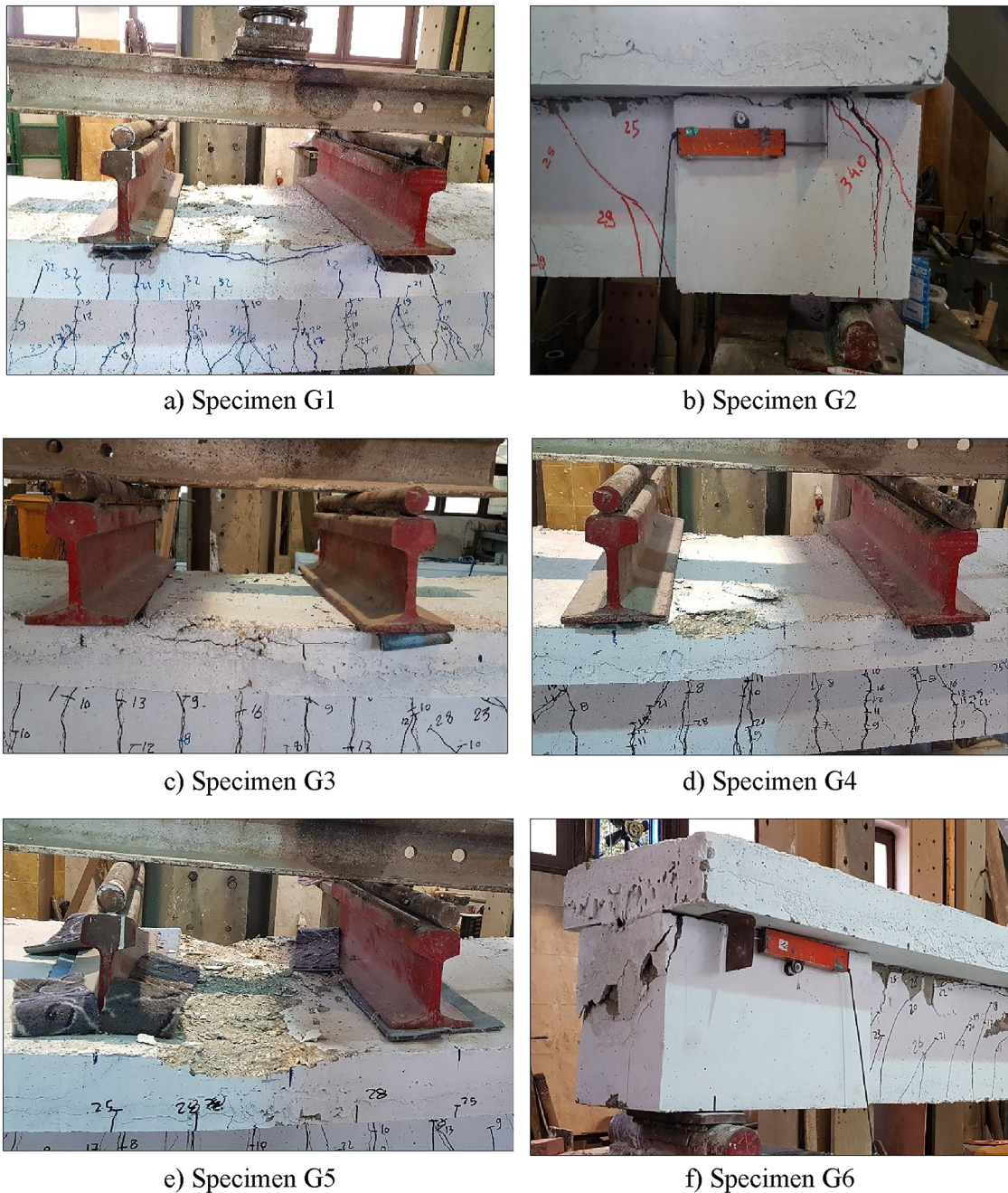


Fig. 20 Failure modes of tested specimens

- Birkeland equation [22]

$$V_n = 2.78 \sqrt{\rho_v f_y} \quad (MPa) \quad (2)$$

- Mattock equation [23]

$$V_n = C + 0.8(\rho_v f_y + \sigma_n) \quad (MPa) \quad (3)$$

Where C=1.38, $\sigma_n=0$

- Shaikh equation [24]

$$V_n = \lambda \sqrt{6.9 \phi \cdot \rho_v \cdot f_y} \leq 0.25 f_c \lambda^2 \text{ and } 6.9 \lambda^2 \quad (MPa) \quad (4)$$

where λ is the constant used to account for the effect of concrete density ($\lambda = 1$) for normal weight concrete, and ϕ is the strength reduction factor for shear ($\phi = 0.85$).

- Loov equation [26]

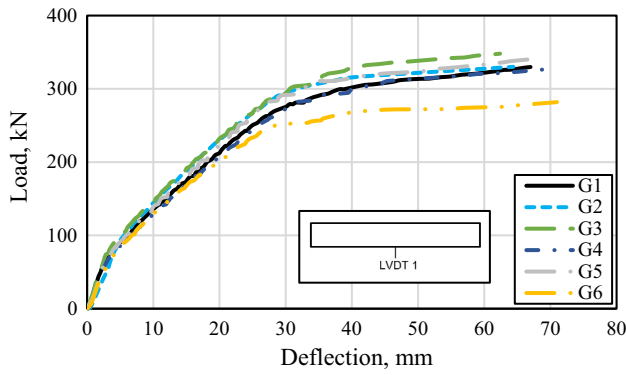


Fig. 21 Load–vertical deflection relationship at LVDT 1

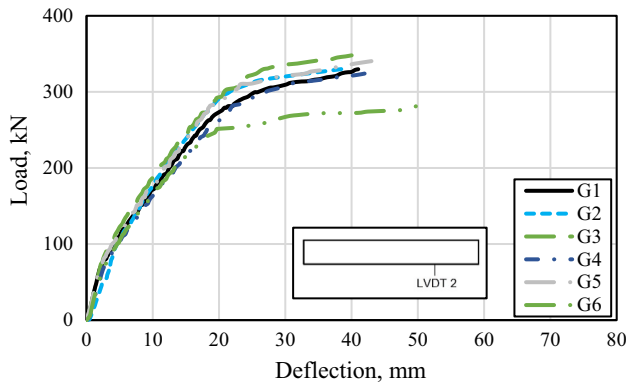


Fig. 22 Load–vertical deflection relationship at LVDT 2

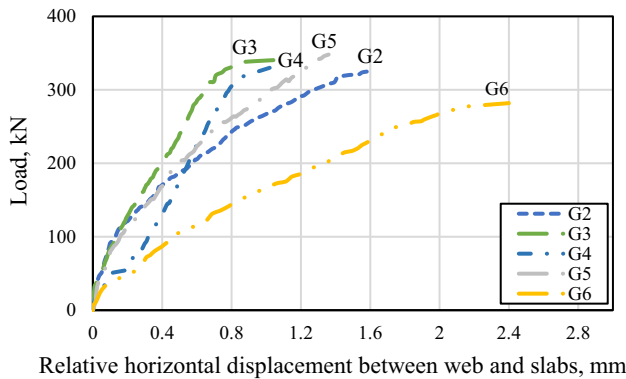


Fig. 23 Load–relative horizontal displacement relationship

$$V_n = k\sqrt{\rho_v f_y f_c} \text{ (MPa)} \tag{5}$$

where k is constant ($k = 0.5$ was suggested for an initially un-cracked interface).

- Patnaik equation [27]

$$V_n = C + \rho_v f_y \leq 0.2f_c \text{ and } 5.5 \text{ MPa} \tag{6}$$

where $C = 0.60$

- AASHTO LRFD 2010 [28]

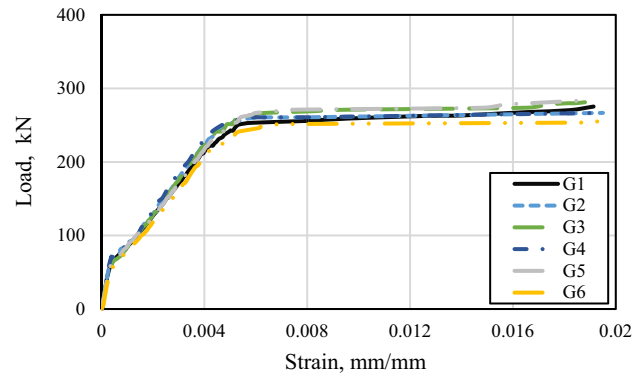


Fig. 24 Load–longitudinal strain relationship at the mid-span

$$V_n = C + \mu \cdot \rho_v \cdot f_y \text{ (MPa)} \tag{7}$$

where $C = 1.90, \mu = 1$

- Eurocode-2 [29]

$$V_n = C f_{ct} + \mu \cdot \rho_v \cdot f_y \text{ (MPa)} \tag{8}$$

where $C = 0.77, \mu = 0.60$

- ECP203-2020 [30]

$$V_n = 1.35 + 0.5 \cdot \rho_v \cdot f_y \text{ (MPa)} \tag{9}$$

- BS 8110–1997 [31]

$$V_n = \rho_v \cdot f_y \tag{10}$$

Where V_n is the ultimate horizontal shear stress, P_{ver} is the vertical ultimate load (theoretical), and P_{exp} is the experimental failure load.

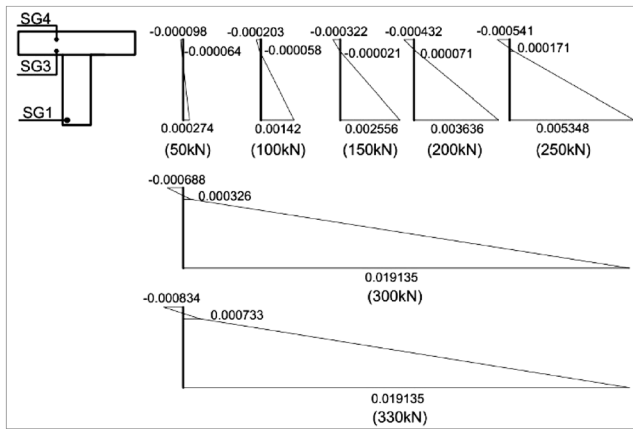
(% Con. = (% Conservatism))

$$= \frac{(\text{Experimental result} - \text{Analysis result})}{\text{Analysis result}} \times 100$$

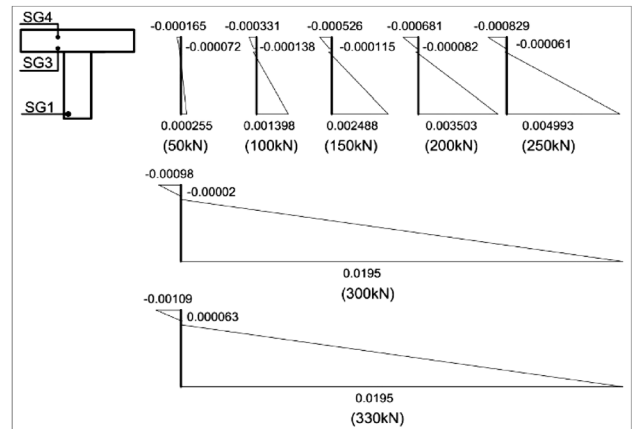
6 Summary and Conclusions

The current study tested six composite T-girders to evaluate the composite behaviour of post tensioned precast concrete girders with top slabs. The bottom slab is precast, and the top part is cast in place. Among the variables studied were the distribution of shear connectors, the extension of girder stirrups to act as shear connectors, the top slab’s width, and the compressive concrete strength of the top slabs. The following conclusions are summarized in the following paragraphs.

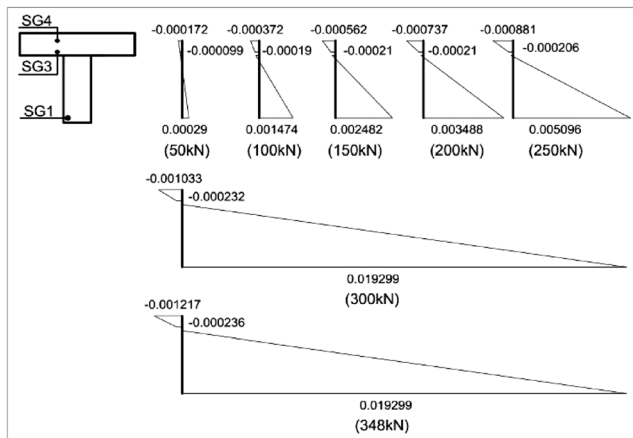
Shear connectors are used to connect the top slabs to the girders. This achieves almost the full composite action as the monolithic T-section girder since the shear connectors can provide the ultimate horizontal shear strength at the interface of the top slabs and the girders. For the same



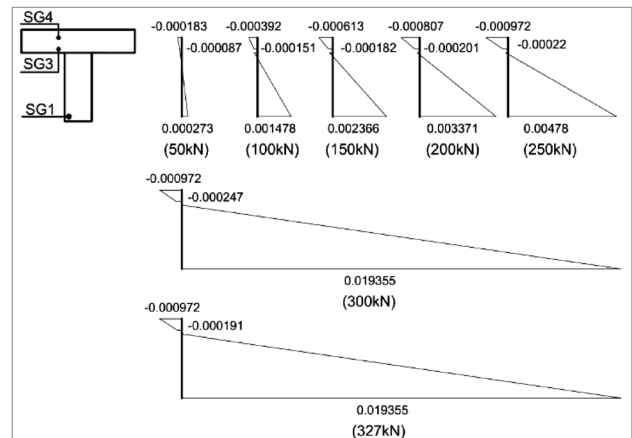
a) Strain Distribution for Specimen G1



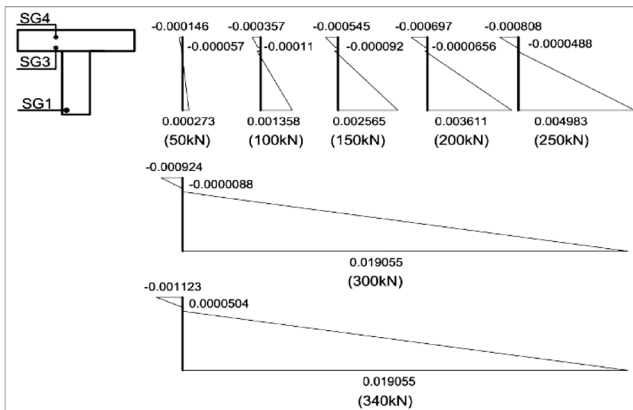
b) Strain Distribution for Specimen G2



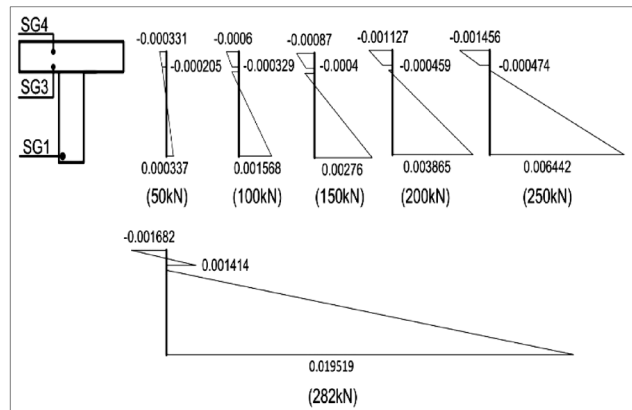
c) Strain Distribution for Specimen G3



d) Strain Distribution for Specimen G4



e) Strain Distribution for Specimen G5



f) Strain Distribution for Specimen G6

Fig. 25 Strain distributions

shear connector reinforcement ratio, the larger diameter of shear connectors shows higher capacity than the smaller diameter due to the higher stiffness of the larger bars.

Shear connectors of 10 mm diameter achieved 100% of the monolithic T-section girder. However, failure occurred

due to slippage between the girder and topping slab while using shear connectors of 12 mm diameter achieved 105% of the monolithic T-section girder and failure occurred as the monolithic T-section girder.

Table 3 Considered variables in the different analytical models

Variable	Mast [21]	Birkland [22]	Mattock [23]	Shaikh [24]	Loov [26]	Patnaik [27]	AASHTO [28]	Eurocode-2 [29]	ECP [30]	BS [31]
f_c	N	N	N	N	Y	N	N	N	N	N
f_y	Y	Y	Y	Y	Y	Y	Y	Y	Y	Y
ρ_v	Y	Y	Y	Y	Y	Y	Y	Y	Y	Y
μ	Y	N	Y	Y	N	Y	Y	Y	Y	N
C	N	N	Y	N	N	Y	Y	Y	Y	N

*Y: yes, *N: no

Table 4 Comparison of experimental results versus using equations of previous researchers and design codes

Equation	Girder ID	f_c (MPa)	f_y (MPa)	ρ_v %	μ	C	V_n (MPa)	$P_{ver..}$ (kN)	$P_{exp.}$ (kN)	$P_{exp.}/P_{ver..}$	% Con
Mast equation [21]	G2	–	400	0.405	1	–	1.62	140.02	330	2.36	135.68
	G3	–	400	0.405	1	–	1.62	139.59	348	2.49	149.29
	G4	–	240	0.698	1	–	1.68	144.76	327	2.26	125.88
	G5	–	400	0.405	1	–	1.62	140.02	340	2.43	142.82
	G6	–	400	0.405	1	–	1.62	140.02	282	2.01	101.40
	Birkland equation [22]	G2	–	400	0.405	–	–	3.54	305.77	330	1.08
G3		–	400	0.405	–	–	3.53	305.31	348	1.14	13.98
G4		–	240	0.698	–	–	3.60	310.91	327	1.05	5.18
G5		–	400	0.405	–	–	3.54	305.77	340	1.11	11.19
G6		–	400	0.405	–	–	3.54	305.77	282	0.92	– 7.78
Mattock equation [23]		G2	–	400	0.405	0.8	1.38	2.68	231.25	330	1.43
	G3	–	400	0.405	0.8	1.38	2.67	230.91	348	1.51	50.71
	G4	–	240	0.698	0.8	1.38	2.72	235.04	327	1.39	39.12
	G5	–	400	0.405	0.8	1.38	2.68	231.25	340	1.47	47.03
	G6	–	400	0.405	0.8	1.38	2.68	231.25	282	1.22	21.95
	Shaikh equation [24]	G2	–	400	0.405	–	–	3.08	266.37	330	1.24
G3		–	400	0.405	–	–	3.08	265.97	348	1.31	30.84
G4		–	240	0.698	–	–	3.13	270.85	327	1.21	20.73
G5		–	400	0.405	–	–	3.08	266.37	340	1.28	27.64
G6		–	400	0.405	–	–	3.08	266.37	282	1.06	5.87
Loov equation [26]		G2	34	400	0.405	–	–	3.71	320.68	330	1.03
	G3	34	400	0.405	–	–	3.71	320.18	348	1.09	8.69
	G4	34	240	0.698	–	–	3.77	326.06	327	1.00	0.29
	G5	34	400	0.405	–	–	3.71	320.68	340	1.06	6.03
	G6	21.25	400	0.405	–	–	2.93	253.52	282	1.11	11.24
	Patnaik equation [27]	G2	–	400	0.405	1	0.6	2.22	191.86	330	1.72
G3		–	400	0.405	1	0.6	2.22	191.43	348	1.82	81.79
G4		–	240	0.698	1	0.6	2.28	196.60	327	1.66	66.32
G5		–	400	0.405	1	0.6	2.22	191.86	340	1.77	77.21
G6		–	400	0.405	1	0.6	2.22	191.86	282	1.47	46.98

Table 4 (continued)

Equation	Girder ID	f_c (MPa)	f_y (MPa)	ρ_v %	μ	C	V_n (MPa)	$P_{ver..}$ (kN)	$P_{exp.}$ (kN)	$P_{exp.}/P_{ver..}$	% Con
AASHTO LRFD 2010 [28]	G2	–	400	0.405	1	1.9	3.52	304.18	330	1.08	8.49
	G3	–	400	0.405	1	1.9	3.52	303.75	348	1.15	14.57
	G4	–	240	0.698	1	1.9	3.58	308.92	327	1.06	5.85
	G5	–	400	0.405	1	1.9	3.52	304.18	340	1.12	11.77
	G6	–	400	0.405	1	1.9	3.52	304.18	282	0.93	– 7.29
	Eurocode-2 [29]	G2	–	400	0.405	0.6	0.77	1.74	150.54	330	2.19
G3		–	400	0.405	0.6	0.77	1.74	150.28	348	2.32	131.56
G4		–	240	0.698	0.6	0.77	1.78	153.39	327	2.13	113.19
G5		–	400	0.405	0.6	0.77	1.74	150.54	340	2.26	125.85
G6		–	400	0.405	0.6	0.77	1.74	150.54	282	1.87	87.32
ECP203–2020 [30]		G2	–	400	0.405	0.5	1.35	2.16	186.65	330	1.77
	G3	–	400	0.405	0.5	1.35	2.16	186.44	348	1.87	86.66
	G4	–	240	0.698	0.5	1.35	2.19	189.02	327	1.73	73.00
	G5	–	400	0.405	0.5	1.35	2.16	186.65	340	1.82	82.16
	G6	–	400	0.405	0.5	1.35	2.16	186.65	282	1.51	51.08
	BS 8110–1997 [31]	G2	–	400	0.405	–	–	1.62	140.02	330	2.36
G3		–	400	0.405	–	–	1.62	139.59	348	2.49	149.29
G4		–	240	0.698	–	–	1.68	144.76	327	2.26	125.88
G5		–	400	0.405	–	–	1.62	140.02	340	2.43	142.82
G6		–	400	0.405	–	–	1.62	140.02	282	2.01	101.40

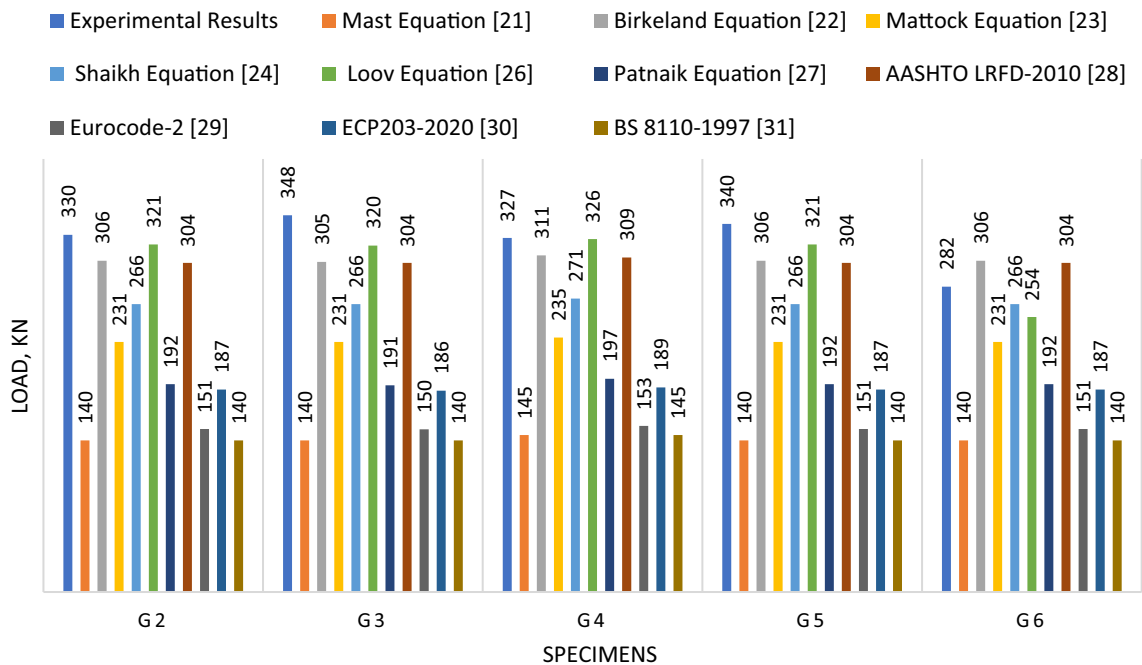


Fig. 26 Comparison between experimental results and previous research and codes

Extending girder stirrups to connect the top slabs to the girders instead of using shear connectors, achieved almost the full composite action as the monolithic T-section girder, and shows better ductility compared with using the shear connectors. Increasing the top slab width by 50% leads to increasing the capacity of the girder with ratio 3% and improved the ductility of the composite T-girder.

Reducing the concrete strength of topping slabs from 40 to 25 MPa leads to decreasing the ultimate capacity of the girder by 15% and increasing slippage between top slabs and girders.

It was found that predicting equations of Mast [21], BS 8110 [31], Eurocode-2 [29], ECP 203–2020 [30], and Patnaik [27] represent the most conservative equations for determining horizontal shear stress due to the conservative values for cohesion and interfacial friction. Equations of Mattock [23] and Shaikh [24] provide moderate conservative equations for determining the horizontal shear stress due to the high contribution of cohesion and friction in those equations. Equations of Loov [26], Birkeland [22], and AASHTO LRFD [28] represent the least conservative equation.

Acknowledgements The experimental program was carried out at the concrete laboratory, Faculty of Engineering, Ain Shams University. Technicians and lab staff are acknowledged for their great help with day-to-day problems.

Funding The authors state that they did not get any funding for this research, and it is self-funded.

Declarations

Conflict of interest The authors declare that they have no conflict of interest.

Human and animal participants This article does not contain any studies with human participants or animals performed by any of the authors.

References

- Issa MA, Salas JS, Shabila HI, Alrousan RZ (2006) Composite behavior of precast concrete full-depth panels and prestressed girders. *PCI J* 51(5):132. <https://doi.org/10.15554/pcij.09012006.132.145>
- Menkulasi F, Roberts-Wollmann CL (2005) Behavior of horizontal shear connections for full-depth precast concrete bridge decks on prestressed I-girders. *PCI J* 50(3):60–73. <https://doi.org/10.15554/pcij.05012005.60.73>
- Farzad M, Shafieifar M, Azizinamini A (2019) Experimental and numerical study on bond strength between conventional concrete and ultra high-performance concrete (UHPC). *Eng Struct* 186:297–305. <https://doi.org/10.1016/j.engstruct.2019.02.030>
- Tawadrous R, Morcou G (2019) Design of shear pocket connection in full-depth precast concrete deck systems. *Eng Struct* 179:367–386. <https://doi.org/10.1016/j.engstruct.2018.11.003>
- Tawadrous R, Morcou G (2018) Interface shear resistance of clustered shear connectors for precast concrete bridge deck systems. *Eng Struct* 160:195–211. <https://doi.org/10.1016/j.engstruct.2018.01.007>
- Leblouba M, Barakat S, Ahmed MSA, Al-Toubat S (2019) Shear strength at the interface of precast bridge concrete decks and girders subjected to cyclic loading with varying speeds. *Eng Struct* 196:109296. <https://doi.org/10.1016/j.engstruct.2019.109296>
- Kamar A, Lasheen M, Shaat A, Zaher A, Khalil A (2021) Factors affecting slip and stress distribution of concrete slabs in composite beams. *Eng Struct* 245:112880. <https://doi.org/10.1016/j.engstruct.2021.112880>
- Keo P, Lepourry C, Somja H, Palas F (2018) Behavior of a new shear connector for U-shaped steel-concrete hybrid beams. *J Constr Steel Res* 145:153–166. <https://doi.org/10.1016/j.jcsr.2018.01.028>
- Abu-Sena AB, Shaaban IG, Soliman MS, Gharib KA-AM (2020) Effect of geometrical properties on strength of externally prestressed steel-concrete composite beams. *Proc Institut Civil Eng-Struct Build* 173(1):42–62. <https://doi.org/10.1680/jstbu.17.00172>
- Jiang H, Fang Z, Liu A, Li Y, Feng J (2016) Interface shear behavior between high-strength precast girders and lightweight cast-in-place slabs. *Construct Build Mater* 128:449–460. <https://doi.org/10.1016/j.conbuildmat.2016.10.088>
- Gao Y, Li C, Wang X, Zhou Z, Fan L, Heng J (2021) Shear-slip behaviour of prefabricated composite shear stud connectors in composite bridges. *Eng Struct* 240:112148. <https://doi.org/10.1016/j.engstruct.2021.112148>
- Rueda-García L, Senach JLB, Sosa PFM, Prada MÁF (2021) Experimental analysis of the shear strength of composite concrete beams without web reinforcement. *Eng Struct* 229:111664. <https://doi.org/10.1016/j.engstruct.2020.111664>
- Rueda-García L, Senach JLB, Sosa PFM, Prada MÁF (2022) Experimental study on the shear strength of reinforced concrete composite T-shaped beams with web reinforcement. *Eng Struct* 225:113921. <https://doi.org/10.1016/j.engstruct.2022.113921>
- Gohnert M (2003) Horizontal shear transfer across a roughened surface. *Cement Concr Compos* 25(3):379–385. [https://doi.org/10.1016/S09589465\(02\)00050-1](https://doi.org/10.1016/S09589465(02)00050-1)
- Xia J, Shan K, Wu X, Gan R, Jin W (2021) Shear-friction behavior of concrete-to-concrete interface under direct shear load. *Eng Struct* 238:112211. <https://doi.org/10.1016/j.engstruct.2021.112211>
- Haber ZB, Munoz JF, De la Varga I, Graybeal BA (2018) Bond characterization of UHPC overlays for concrete bridge decks: Laboratory and field testing. *Constr Build Mater* 190:1056–1068. <https://doi.org/10.1016/j.conbuildmat.2018.09.167>
- Liu J, Chen Z, Guan D, Lin Z, Guo Z (2020) Experimental study on interfacial shear behaviour between ultra-high performance concrete and normal strength concrete in precast composite members. *Construct Build Mater* 261:120008. <https://doi.org/10.1016/j.conbuildmat.2020.120008>
- Zhang Y, Zhu P, Wang X, Wu J (2020) Shear properties of the interface between ultra-high performance concrete and normal strength concrete. *Construct Build Mater* 248:118455. <https://doi.org/10.1016/j.conbuildmat.2020.118455>
- Semendary AA, Hamid WK, Steinberg EP, Khoury I (2020) Shear friction performance between high strength concrete (HSC) and ultra high performance concrete (UHPC) for bridge connection applications. *Eng Struct* 205:110122. <https://doi.org/10.1016/j.engstruct.2019.110122>
- Huang H, Yuan Y, Zhang W, Gao Z (2019) Bond behavior between lightweight aggregate concrete and normal weight

- concrete based on splitting-tensile test. *Constr Build Mater* 209:306–314. <https://doi.org/10.1016/j.conbuildmat.2019.03.125>
21. Mast RF (1968) Auxiliary reinforcement in concrete connections. *J Struct Div* 94(6):1485–1504. <https://doi.org/10.1061/JSDEAG.0001977>
 22. Birkeland PW, Birkeland HW (1966) Connections in precast concrete construction. *ACI Struct J* 63(3):345–368
 23. Mattock AH, Hawkins NM (1972) Shear transfer in reinforced concrete-recent research. *PCI J* 17(2):55–75. <https://doi.org/10.15554/pcij.03011972.55.75>
 24. Shaikh AF (1978) Proposed revisions to shear-friction provisions. *PCI J* 23(2):12–21
 25. ACI Committee 318–19 (2019) Building code requirements for structural concrete (ACI 318–19) and commentary (318R–19). American Concrete Institute, Farmington Hills
 26. Loov RE, Patnaik AK (1994) Horizontal shear strength of composite concrete beams with a rough interface. *PCI J* 39(1):48–69. <https://doi.org/10.15554/pcij.01011994.48.69>
 27. Patnaik AK (2001) Behavior of composite concrete beams with smooth interface. *J Struct Eng* 127(4):359–366. [https://doi.org/10.1061/\(ASCE\)0733-9445\(2001\)127:4\(359\)](https://doi.org/10.1061/(ASCE)0733-9445(2001)127:4(359))
 28. AASHTO (2010) AASHTO LRFD Bridge Design Specifications, Customary U.S. Units. American Association of State Highway and Transportation Officials, Washington, DC
 29. Eurocode-2 (2004) European Committee for standardization, EN 1992–1–1, Design of Concrete Structures – Part 1–1: General Rules and Rules for Buildings. European Committee
 30. ECP 203–2020 (2020) Egyptian Building Code for Structural Concrete Design and Construction. Ministry of Housing, Utilities and Urban Communities, Cairo.
 31. British Standards Institution (1997) BS 8110, part 1: structural use of concrete: code of practice for design and construction. BSI, London